JOURNAL OF APPLIED ELECTROCHEMISTRY **28** (1998) 173–183

# Electrodissolution of iron in sodium sulfate and sodium bicarbonate solutions at pH 8

G. VATANKHAH, M. DROGOWSKA, H. MENARD

*Chemistry Department, Sherbrooke University, Sherbrooke, Québec, Canada J1K 2R1*

L. BROSSARD

*Institut de recherche d'Hydro-Québec, 1800 Boul. Lionel-Boulet, Varennes, Québec, Canada J3X 1S1*

Received 22 July 1996; revised 27 March 1997

The effect of sulfate ions on the electrochemical behaviour of iron electrodes in the presence of bicarbonate ions has been investigated. In solutions containing sulfate ions only, iron electrodes experience uniform corrosion and sulfate ions are aggressive. In the presence of bicarbonate ions, the sulfate ions become less aggressive and a pitting–repassivation process is observed. The differences in electrochemical behaviour have been compared and explained by examining the formation of probable products and their physicochemical properties during electrochemical polarization.

Keywords: *iron*, *sulfate ions*, *pitting*, *repassivation*, *electrodissolution*

## 1. Introduction

The available literature on the pitting corrosion of iron and its alloys is mainly focused on the effect of chloride ions [1–8]. By contrast, the literature for pitting by sulfate ions is scarce [9–16]. Although it has been considered that $Cl^-$ ions are more aggressive than other anions, the effect of $SO_4^{2-}$ ions is probably seen most frequently because of their stability in water over a wide range of pH ($\geq 2$). It has been reported that pitting induced by sulfate ions on iron occurs within the active–passive region and sulfate ions may counteract the effect of chloride ions [12, 13].

The film breakdown potential of iron in the presence of chloride or sulfate ions obeys the logarithmic behaviour with the difference that with sulfate ions the mechanism of pitting changes over time [9]. Ellipsometric measurements of film grown on iron in a borate buffer solution containing sulfate ions, revealed a different structure of the surface film in the potential range with and without pitting [14]. MacDougall and Bardwell [15] have shown that in sulfate solutions of pH 3.0 or 8.4, the passivation is highly inefficient with a very large anodic charge prior to a substantial decrease in current. They concluded that passivation (in these solutions) appears to be associated with the precipitation of a salt film and/or changes in the solution pH near the surface, thus allowing a passive oxide to form.

Recently, the considerable influence of pH on the passive film formed on iron in a $Na_2SO_4$ solution was shown [16] through the use of surface enhanced Raman spectroscopy (SERS). At pH 10, the passive film consists of microcrystalline/amorphous $Fe(OH)_2$ + $Fe_3O_4$ and/or $\gamma$-$Fe_2O_3$, with the sulfate anions being adsorbed on the film surface. Sulfate ions are incorporated into the film and bind covalently with the iron cations at pH 5.

Acosta *et al.* [17] have investigated the effect of sulfate ions on the pitting corrosion of mild steel in phosphate–borate solutions in a potential region from $-1.0$ to 0.0 V vs SCE. A linear relationship between the logarithm of the sulfate ion concentration and the breakdown potential $E_b$ is reported, with the pitting process being limited to a narrow potential range in the passive region due to the existence of an inhibition process.

To our knowledge, the only available data for the electrochemical behaviour of iron in a mixture of sulfate and bicarbonate ions is from Pound *et al.* [18]. They have reported one voltammogram only for iron in a solution of 1 M sodium sulfate +0.003 M sodium bicarbonate and a scan rate of 50 mV $s^{-1}$ from $-1$ to 0.8 V vs SHE. A broad anodic peak located at $-0.9$ V with a maximum peak current density of 60 mA $cm^{-2}$ along with a small conjugated cathodic peak at $-0.15$ V were observed. The large anodic peak is linked to a dissolution reaction.

Génin *et al.* [19–26] published a series of articles on *E*–pH diagrams of iron in different solutions of sulfate, chloride, carbonate/bicarbonate, and their mixtures. They considered both thermodynamically and experimentally the existence of green rusts, which are very important corrosion transient products in such media. Their results are very useful for interpreting data obtained for the study of pitting corrosion by chloride and sulfate ions.

The present investigation pertains to the electrochemical characterization of iron in sulfate, bicarbonate and sulfate + bicarbonate solutions, with special focus on the effect of sulfate ions. The sulfate and bicarbonate ion concentrations range from 0.3

 © 1998 Chapman & Hall 

to 1 M and 0.01 to 0.5 M, respectively. As far as the potentiodynamic behaviour is concerned, the potential ranges from a hydrogen to an oxygen evolution.

## 2. Experimental details

Working electrodes were made of iron (Johnson Matthey) in a Kel-F holder used as a rotating-disc electrode. The exposed area was 0.13 $cm^2$. The electrodes were mechanically polished with alumina paste to a mirror-like finish and rinsed with distilled water. The electrode surface was examined before and after the experiments using a Bausch and Lomb optical microscope (70×). For each experiment, the electrode was kept at a constant applied potential of −1.0 V vs SCE for 1 min in order to reduce any air-formed surface oxides. The auxiliary electrode was a platinum grid, separated from the main compartment by a Nafion® membrane. The reference electrode was a saturated calomel electrode (SCE) with a Luggin capillary bridge connected to the main cell. All potentials in this paper are reported with respect to the SCE. The rotation speed ($\omega$) of the working electrode was 1000 rpm.

Aqueous solutions of 0.3–1 M $Na_2SO_4$ and 0.1–0.3 M $NaHCO_3$ were prepared from analytical grade materials (BDH) and deionized water. The pH was ~8 for all solutions and no pH adjustment was done. A 600 ml cell was used to minimize the enrichment of the solution in dissolved ions during the experiments. All solutions were deaerated by high-purity nitrogen bubbling before each experiment and were purged continuously during the measurements. All of the experiments were conducted at room temperature.

The instrument used for all the experiments was a potentiostat/galvanostat (model 273) from Princeton Applied Research (PAR) controlled by a PC using M270 PAR electrochemical software version 4.10. Electrode rotation was done using an electrode rotator from Pine instrument company.

## 3. Results

### 3.1. *Sulfate solutions*

A voltammogram of an iron electrode rotated at 1000 rpm with a potential scan rate of 0.005 V $s^{-1}$ from −0.85 to 1.5 V in 1 M $Na_2SO_4$ (pH ~ 8) solution is shown in Fig. 1. The anodic current starts to increase at −0.85 V to reach a maximum of 480 mA $cm^{-2}$ at 0.11 V. The large anodic charge is related to the iron dissolution as Fe(II) [27]. After the peak current, there is a sharp decrease of three orders of magnitude in anodic current to 480 $\mu$A $cm^{-2}$ at 0.25 V and a large quasi-passive region extending over 1 V with a current as low as 50 $\mu$A $cm^{-2}$. In the transpassive region for potentials more anodic than 1.25 V, the oxidation current increases with the potential and oxygen evolution is observed. For the potential scan in the negative direction, the passivation remains up to −0.3 V with a minimum current of 2–3 $\mu$A $cm^{-2}$. There is a small broad anodic current peak maximum of 65 $\mu$A $cm^{-2}$ at −0.3 V, which indicates an activation (dissolution) of the electrode surface. The height and location of the activation peak for the potential sweep in the negative direction are dependent on the anodic potential scan limits (Fig. 2), that is, 0, 0.2 and 0.4 V. The activation current peak maximum is lowered by increasing the anodic potential limit $E_a$; for $E_a \geqslant 0.5$ V, the anodic reactivation peak current disappears and cathodic current is observed. Figure 1 also illustrates the effect of a negative potential scan direction ranging from 1.5 to −0.85 V; the potentio-

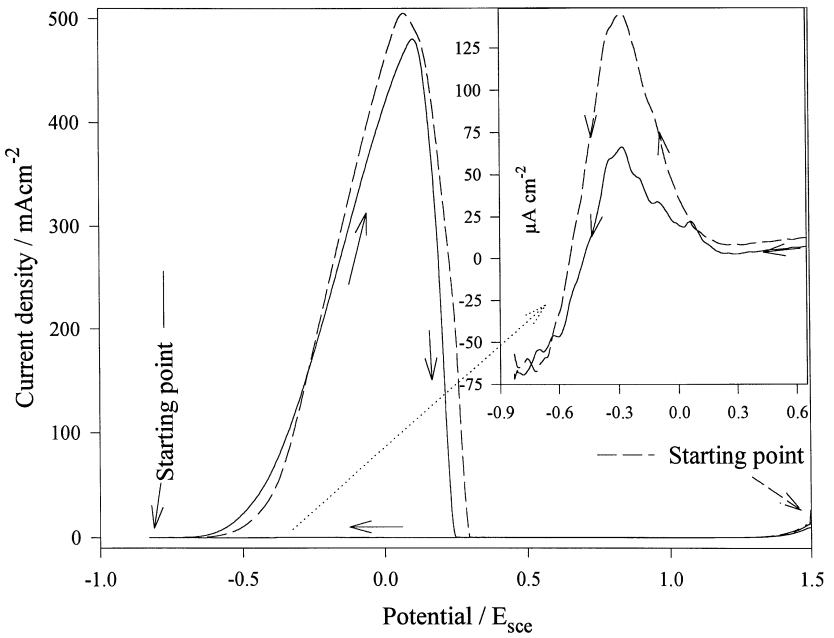


Fig. 1. Potentiodynamic trace for a rotating iron disc electrode, in 1 M sodium sulfate solution, $dE/dt = 5$ mV $s^{-1}$; $\omega = 1000$ rpm; compensated for the *IR* drop. Starting potential: −0.85 V (continuous line); +1.5 V (dashed line).

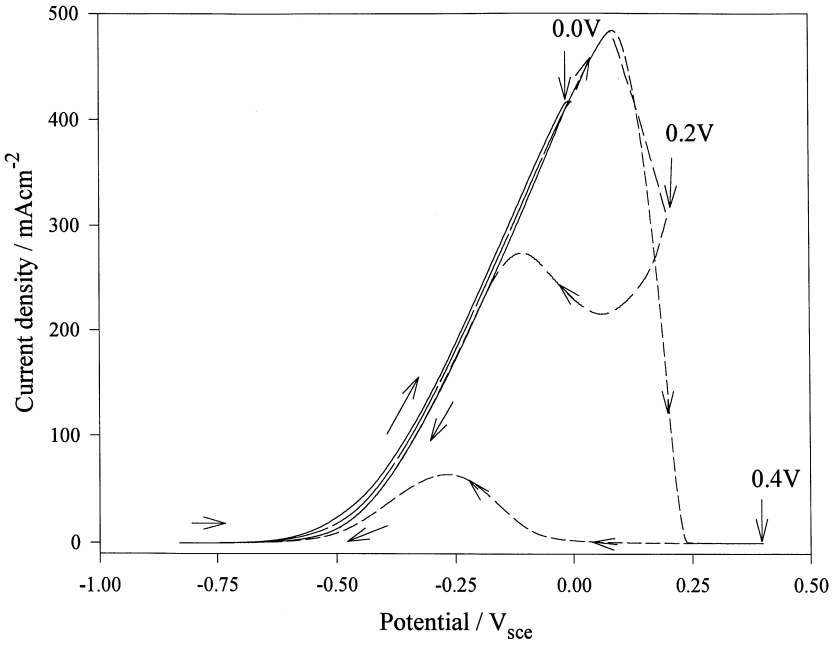


Fig. 2. Effect of the anodic potential limit (0–0.4 V) on the voltammogram during the return sweep. Starting potential: −0.85 V. The other experimental conditions are those of Fig. 1. $E_r^a$ :(——) 0.0, (— —) 0.2 and (– – –) 0.4 V.

dynamic trace overlaps the one with a starting potential of −0.85 V in a positive potential scan direction. At the end of each experiment, it was observed that the electrode surface is etched strongly and looks very rough.

The oxidation current in the passive region is dependent on the sulfate ion concentration, that is, it is equal to 60 $\mu$A cm$^{-2}$ for 1 M $Na_2SO_4$ (Fig. 1) and 110 $\mu$A cm$^{-2}$ for 0.3 M $Na_2SO_4$ at $E = 0.8$ V. For the scan in the negative potential direction, the current from 1 to 0.2 V is independent of the sulfate concentration.

The chronoamperograms for the iron electrode in 0.3 M $Na_2SO_4$ for two different constant applied potentials (i.e., 0.2 V and 0.4 V) are illustrated in Fig. 3, the potential being stepped from −1 to 0.2 or 0.4 V. The current is anodic with peaks and spikes related to pitting. For $E = 0.2$ V, the curve displays an anodic current maximum for Fe(II) dissolution after about 600 s of polarization; for a longer time, the anodic current decreases over time to reach a quasi-steady value of 140 $\mu$A cm$^{-2}$ for $t = 3200$ s. For $E = 0.4$ V, a passivation current of 100 $\mu$A cm$^{-2}$ is attained quickly to reach 16 $\mu$A cm$^{-2}$ after 2000 s. SEM pictures of the electrode surface after 8000 s of polarization under the experimental conditions of Fig. 3 are shown in Figs 4 and 5. The sample maintained at 0.2 V (Fig. 4) shows a large number of pits without any precipitate

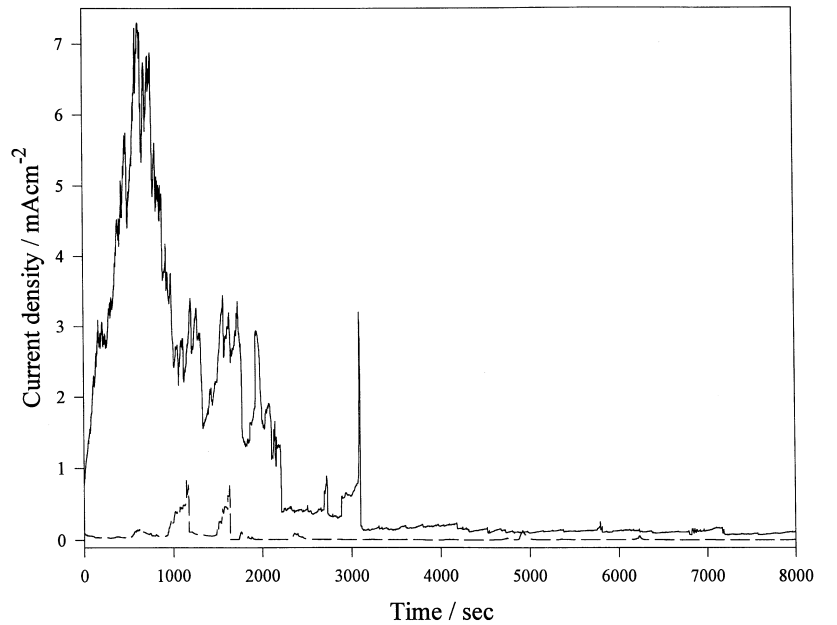


Fig. 3. Current–time curve for an iron electrode in 0.3 M sodium sulfate solution for applied potentials of 0.2 and 0.4 V; $\omega = 1000$ rpm. Key: (——) 0.2 V and (– – –) 0.4 V.

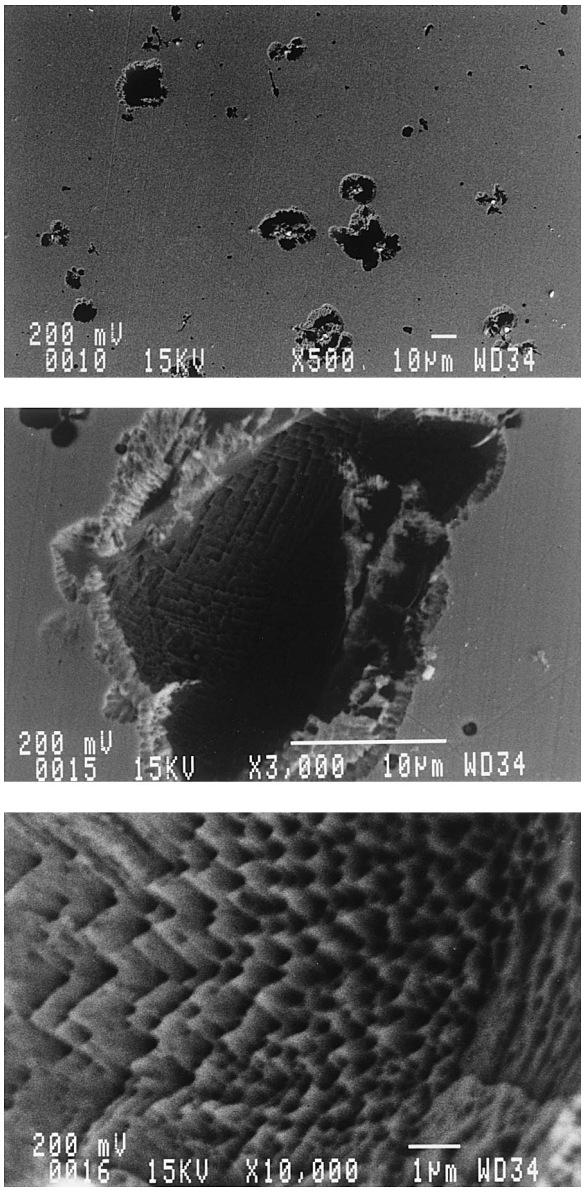


Fig. 4. SEM pictures after iron electrode oxidation at 0.2 V for 8000 s in 0.3 M sodium sulfate solution; $\omega = 1000$ rpm.

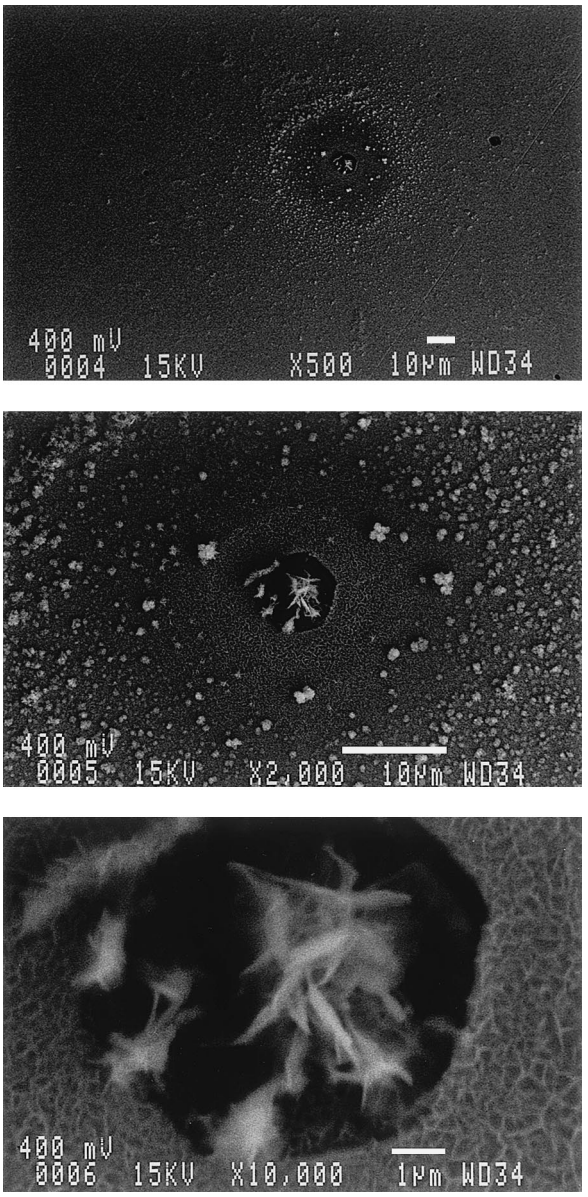


Fig. 5. SEM pictures after electrode oxidation at 0.4 V for 8000 s in 0.3 M sodium sulfate solution; $\omega = 1000$ rpm.

on the electrode surface. For $E = 0.4$ V (Fig. 5), few pits are noticed with a precipitate inside and outside the pits. A further increase of the anodic potential up to 1 V results in a passive current of 20 $\mu$A cm$^{-2}$ and a shiny golden coloured surface after 2000 s is obtained.

### 3.2. *Bicarbonate solutions*

The potentiodynamic behaviour of a rotating iron electrode in 0.1 M $NaHCO_3$ solution (pH $\sim$ 8) has been investigated (Fig. 6) under the experimental conditions of Fig. 1. The potentiodynamic trace in the anodic direction displays an anodic active dissolution peak (region A) with a peak current of 190 $\mu$A cm$^{-2}$ at $-0.64$ V, which is followed by a large passive region from $-0.4$ to 0.9 V (region B). For potentials more positive than 0.9 V, that is, the transpassive region (region C), the anodic current increases with the potential and a plateau current from 1.1 to 1.3 V is observed before the onset of oxygen evolution. The current plateau in the transpassive region is related to oxidation of Fe(III) to Fe(VI) species [28–30]. The anodic peak current in region A and the anodic plateau current in region C are higher as the bicarbonate concentration is increased. For the scan in the negative potential direction, the potentiodynamic trace is unchanged in the plateau region and a single cathodic peak is noticed at $-0.72$ V. The oxidation charge related to the oxidation peak in region A is much larger than its conjugated cathodic peak current.

### 3.3. *Solutions with bicarbonate and sulfate ions*

The voltammogram of a rotating iron disc electrode in 0.3 M $Na_2SO_4$ + 0.01 M $NaHCO_3$ solution obtained under the experimental conditions of Fig. 1 is illustrated in Fig. 7. For the scan in the anodic potential direction, the following features have been noticed: (i) a small anodic peak current (peak I) located at

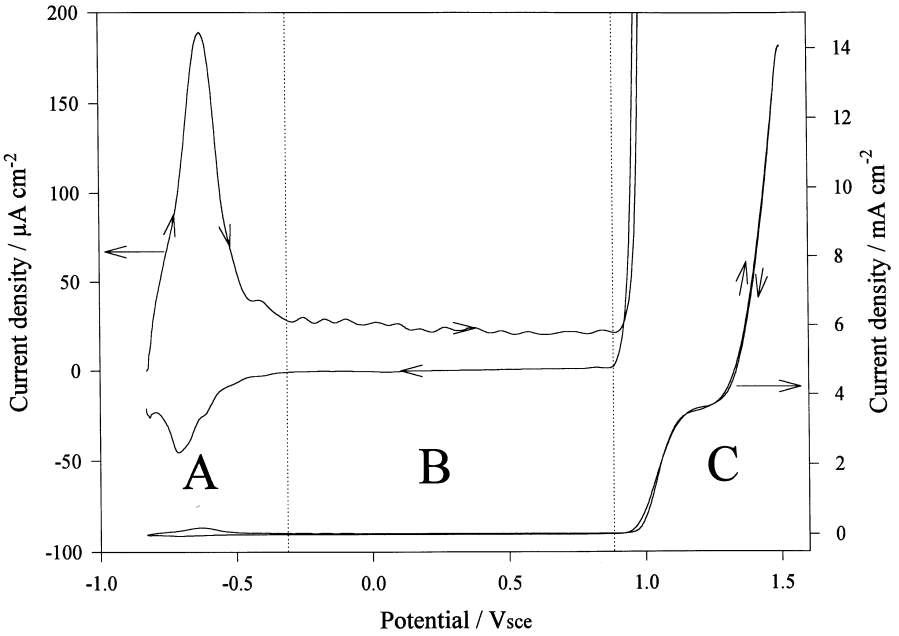


Fig. 6. Potentiodynamic trace for an iron electrode in 0.1 M sodium bicarbonate solution and a scan rate of 5 mV $s^{-1}$. Potential scan limits: −0.85 V and 1.5 V; $\omega = 1000$ rpm.

−0.6 V, (ii) a second, dominant anodic peak current (peak II) with its maximum close to 0 V, and (iii) a passive region extending from 0.4 to 0.9 V, which is followed by a transpassive region prior to the onset of the oxygen evolution at potentials higher than 1.0 V. The electrode surface remains passive for the potential scan reversal and a broad cathodic peak current at −0.75 V is observed. The presence of peak I and the plateau current in the transpassive region is associated with the effect of dissolved $NaHCO_3$ (Fig. 6). The anodic current peak II and the pit formation, which is manifested by small anodic current oscillations close to the peak potential, are induced by the presence of sulfate ions. In Fig. 8 the voltammograms with increasing positive potential limits, that is, −0.35, −0.325 and −0.3 V, illustrate the growth of initial pits by an increase in current for the scan reversal, with the protection potential being close to −0.52 V.

With an increase in the bicarbonate concentration, the sulfate ions concentration being constant, the height of peak current I increases, peak current II decreases and there is an increase in the plateau current in the transpassive region (Fig. 9). With an increase in the sulfate concentration, the concentration in sodium bicarbonate being constant, the anodic current peaks I and II and the current in the passive region increase but the plateau current in the

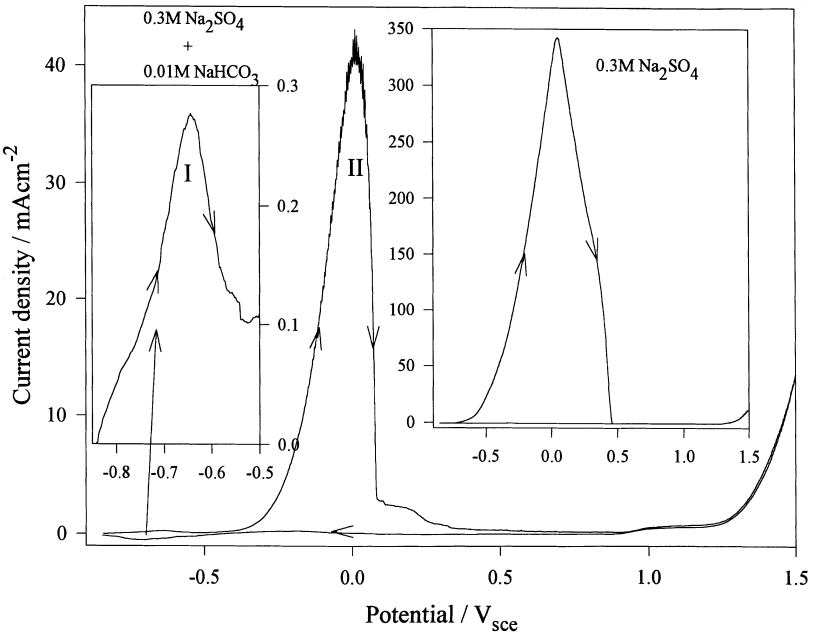


Fig. 7. Potentiodynamic trace for an iron electrode in a solution containing 0.3 M sulfate + 0.01 M bicarbonate, *IR* drop compensated. Insert: 0.3 M sodium sulfate solution only. $dE/dt = 5$ mV $s^{-1}$; $\omega = 1000$ rpm. Potential scan limits: −0.85 V and 1.5 V.

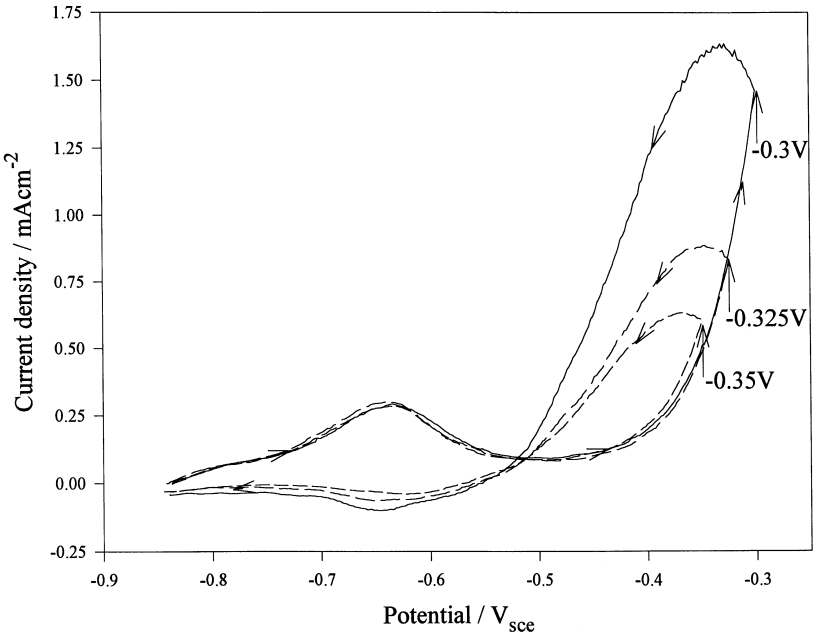


Fig. 8. Effect of switching potentials on the potentiodynamic trace during the return sweep for a solution containing 0.3 M sulfate + 0.01 M biocarbonate. The other experimental conditions are those of Fig. 7.

transpassive region decreases. Peak II is accompanied with pitting corrosion in all cases (Figs 7, 9 and 10). From Figs 9 and 10, it is observed for the reverse potential scan in the region of peak I, that there is more anodic reactivation with an increase in the ratio of sulfate to bicarbonate ions.

The current against time curve for an iron electrode at 0.0 V in 0.1 M $NaHCO_3 + 0.1$ M $Na_2SO_4$ solution is shown in Fig. 11. The current increases over time to reach a quasi steady-state value for iron oxidation after about 150 s. The appearance of the iron surface in the region of the steady-state current remains unchanged over time (Fig. 12). The pictures in Fig. 12 show the formation of a precipitate on the surface during the electrodissolution process.

In another set of experiments (Fig. 13(a)–(d)), the effect of different preoxidation treatments of an iron electrode prior to potentiodynamic characterization in solutions containing bicarbonate ions, sulfate ions, and mixture of both ions was established. For bicarbonate solutions, the iron electrodes have been preoxidized at 0.9 V in 0.1 M $NaHCO_3$ solution to reach an oxidation charge of 500 $\mu$C (4 mC cm$^{-2}$) prior to the potential sweep in the cathodic direction at a scan rate of 0.005 V s$^{-1}$; the potentiodynamic trace is illustrated in Fig. 13(a). In a second set of

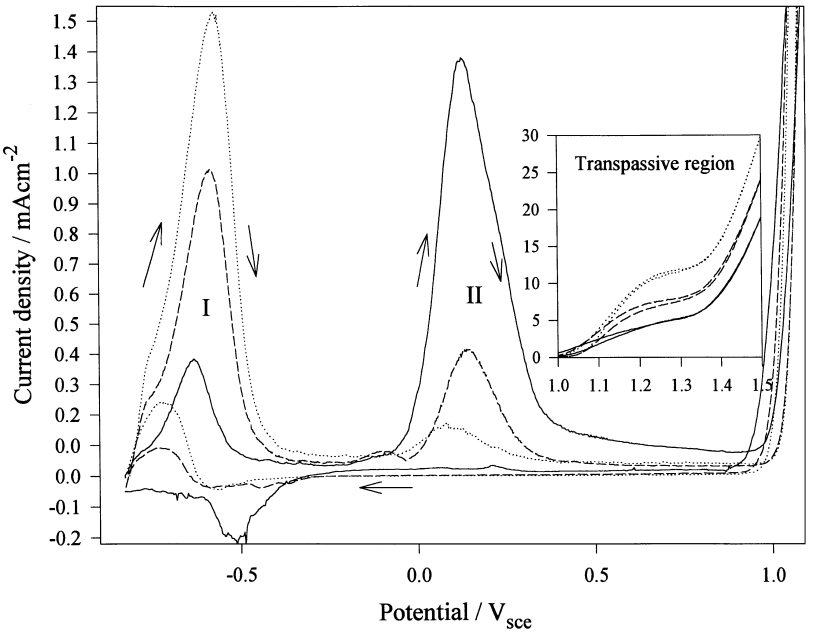


Fig. 9. Voltammograms for an iron electrode in 0.3 M sulfate + $x$ M bicarbonate, $x = 0.1$, 0.3 and 0.5 M; $dE/dt = 5$ mV s$^{-1}$; $\omega = 1000$ rpm; starting potential: −0.85 V. Key: (——) 0.1 M $NaHCO_3$ + 0.3 M $Na_2SO_4$; (– – –) 0.3 M $NaHCO_3$ + 0.3 M $Na_2SO_4$; (·····) 0.5 M $NaHCO_3$ + 0.3 M $Na_2SO_4$.

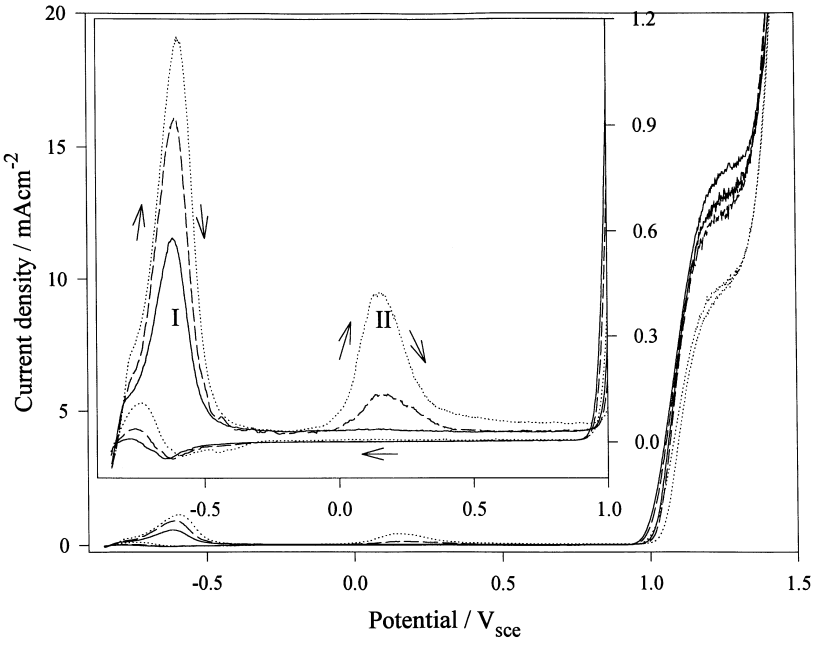


Fig. 10. Voltammograms for an iron electrode in 0.3 M biocarbonate + $x$ M sulfate, $x = 0.1$, 0.3 and 0.5 M; $dE/dt = 5\,mV\,s^{-1}$; $\omega = 1000$ rpm; starting potential: −0.85 V. Key: (——) 0.3 M $NaHCO_3$ + 0.1 M $Na_2SO_4$; (– – –) 0.3 M $NaHCO_3$ + 0.3 M $Na_2SO_4$; (· · · · · ·) 0.3 M $NaHCO_3$ + 0.5 M $Na_2SO_4$.

experiments, the potentiodynamic traces were obtained under the experimental conditions of Fig. 13(a) (including the preoxidation treatment) except that 0.3 M $Na_2SO_4$ was added just prior to the potentiodynamic scan in the cathodic direction (Fig. 13(b)). For a third set of experiments, the electrode has been preoxidized at 0.9 V, to reach an oxidation charge of 500 $\mu$C in the presence of 0.1 M $NaHCO_3$ + 0.3 M $Na_2SO_4$ and then the potentiodynamic trace has been recorded (Fig. 13(c)). For a fourth set of experiments, potentiodynamic traces in the solution containing 0.1 M $NaHCO_3$ + 0.3 M $Na_2SO_4$ without any preoxidation treatment have been recorded (Fig. 13(d)).

In bicarbonate solution only, the potentiodynamic trace (Fig. 13(a)) displays a passivation region up to +0.4 V, a cathodic peak current with its maximum at −0.6 V and an anodic peak current at about −0.7 V. The picture is different with the addition of sulfate ions to the bicarbonate solution (Fig. 13(b)): (i) the oxidation current is bigger at potential values anodic enough, (ii) the current becomes cathodic below about 0.3 V and a plateau current between 0.1 and −0.3 V is noticed and (iii) two consecutive cathodic

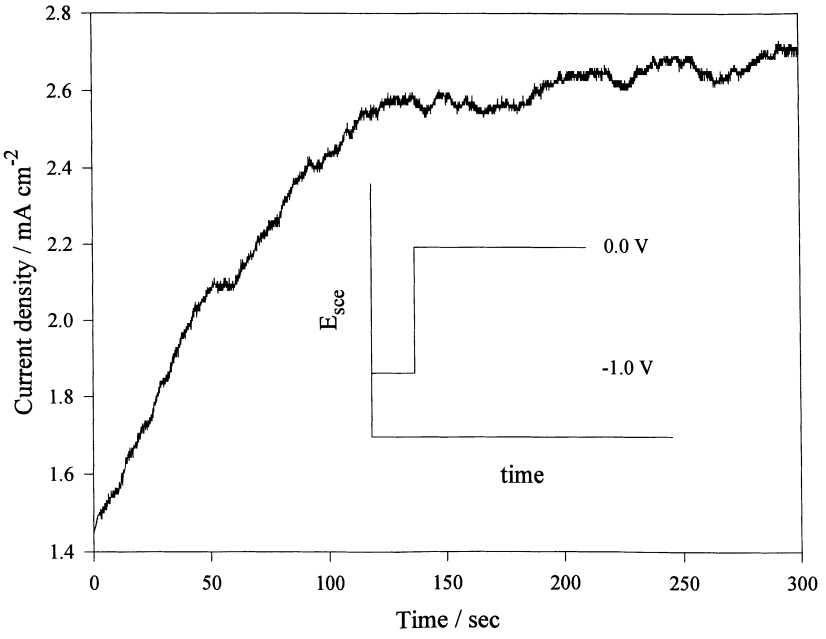


Fig. 11. Chronoamperogram for an iron electrode in a 0.1 M sulfate + 0.1 M bicarbonate solution. $\omega = 1000$ rpm. Insert: applied potential against time.

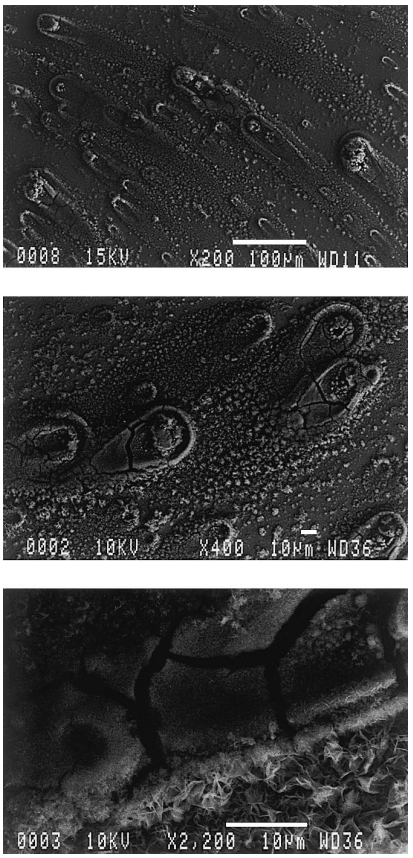


Fig. 12. SEM pictures for an iron electrode after 300 s of oxidation in a 0.1 M sulfate + 0.1 M bicarbonate solution.

peaks located at −0.45 and −0.55 V, respectively, are noted. For 0.1 M $NaHCO_3$ + 0.3 M $Na_2SO_4$ solutions, the potentiodynamic trace (Fig. 13(c)) displays a significant oxidation current up to −0.2 V with two cathodic current peaks, being located at about −0.3 V and −0.55 V. Further, the potentiodynamic trace for an iron electrode without any preoxidation treatment in 0.1 M $NaHCO_3$ + 0.3 M $Na_2SO_4$ (Fig. 13(d)) has approximately the same characteristics as the trace with a preoxidation treatment (Fig. 13(c)), except that the height of the cathodic current peaks at low potentials tends to be lower without preoxidation. In both cases (Fig. 13(c) and (d)), the two cathodic peaks are associated with the reduction of the pitting products and other reducible oxide compounds present on the iron electrode surface.

To determine the critical molar ratio of bicarbonate to sulfate required to avoid any localized attack, experiments have been carried out in the presence of 0.03 and 0.06 M of sulfate plus 0.3 M bicarbonate solutions. The current versus time curve for $E = 0$ V is characterized by pitting corrosion for 0.06 M sulfate and the absence of localized attack for 0.03 M sulfate solutions. The absence of any localized attack for 0.03 M sulfate + 0.3 M bicarbonate has also been noticed for five consecutive potentiodynamic cycles with a scan rate of 0.005 V $s^{-1}$ and $\omega = 1000$ rpm, with the potential limits of −0.85 V and 1.5 V. Compared to cyclic voltammograms obtained in the presence of bicarbonate solutions only (five consecutive cycles), the electrode surface has the same appearance and no localized attack is found. Consequently, it may be deduced that a molar ratio of 10 : 1 of bicarbonate to sulfate results in the complete suppression of any localized attacks induced by the presence of sulfate ions.

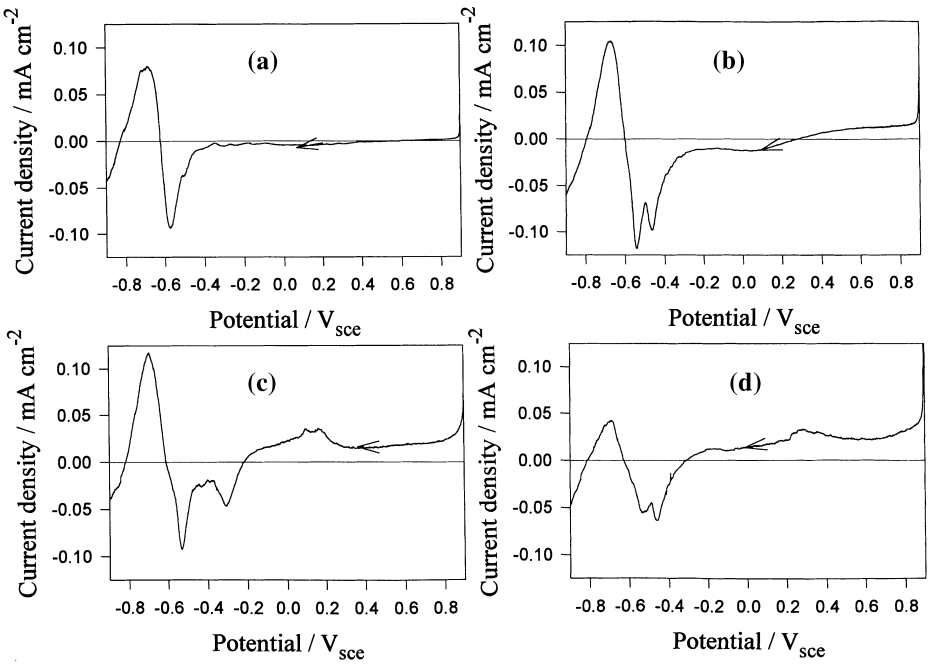


Fig. 13. Voltammograms for an iron electrode: (a) after preoxidation* in 0.1 M bicarbonate solution. Starting potential: 0.9 V, the potential is swept† in the negative direction; (b) after preoxidation* in 0.1 M bicarbonate and the addition of 0.3 M sulfate prior to the potential sweep† in the cathodic direction, starting potential: 0.9 V, (c) after preoxidation* in 0.1 M bicarbonate + 0.3 M sulfate; starting potential: 0.9 V, the potential is swept† in the negative direction, (d) without preoxidation; starting potential: 0.9 V; the potential is swept† in the negative direction, solution: 0.1 M bicarbonate + 0.3 M sulfate. *Preoxidation conditions: $E = 0.9$ V to reach an oxidation charge of 500 $\mu$C (4 mC $cm^{-2}$). †$dE/dt = 5$ mV $s^{-1}$.

## 4. Discussion and conclusions

In the part of the potentiodynamic curve for which the oxidation current increases with the potential for low potentials, the corrosion process is uniform in the presence of $SO_4^{2-}$ ions only and the formation of Fe(II) species is postulated (Fig. 1). The $SO_4^{2-}$ ions participate in the formation of an $FeSO_4$ ion pair complex [31] and the anodic current increases up to a very large value. At more anodic potentials, the large passivation region is explained by a dissolution–precipitation reaction and solid-state oxidation of iron to Fe(II)/Fe(III) oxide/hydroxide [10]. The dark green precipitate observed on the electrode surface is most likely related to a ferrous hydroxy sulfate according to Gibbs and Cohen [32]. Recently, Génin *et al.* [21, 26] proposed, as a transient compound, the green rust 2 (GR2) with the following formula: $4\,Fe(OH)_2.2FeOOH.FeSO_4.nH_2O$ where $n$ is probably 4. The latter compound corresponds to an oxidation number of 2.29 i.e. $5Fe^{2+}$ and $2Fe^{3+}$ ions. At more anodic potentials, the formation of a passive film may be considered according to [26]:

$$4\,Fe(OH)_2.2FeOOH.FeSO_4 + 2\,H_2O = 7\gamma FeOOH + SO_4^{2-} + 7H^+ + 5e^- \qquad (1)$$

When the anodic potential increases from 0.25 to 1.25 V, it is postulated that the hydroxides change to oxides and the Fe(III) oxides may form the passive film. At potentials more anodic than about 1.25 V, a transpassive region is noticed with the oxygen evolution at the potentials that are sufficiently anodic.

The potentiodynamic trace for the potential scan in the negative direction has a passive region as large as 1.55 V (Fig. 1), which is in agreement with the fact that $Fe_2O_3$ is very stable [33]. The minimum passive current in forward (positive) scan ($50\,\mu A\,cm^{-2}$) is large compared to the one of the backward (negative) scan ($2.5\,\mu A\,cm^{-2}$); it is due to the effect of the oxidation potential and time. The passive film is resistant against the sulfate ion attack and the passivation region extends to more negative potentials. At −0.85 V, the cathodic current ($80\,\mu A\,cm^{-2}$) is linked to reduction of an oxides film and hydrogen evolution.

The precipitation of the green rust GR2 is potential and time-dependent, as shown by the potential scan in the negative direction (Fig. 2). The surface oxidation at positive potentials in the presence of sulfate ions induces the formation of a passive film but the precipitation of a sulfate product alone can not protect the electrode against localized attack or uniform electrodissolution.

The effect of the applied potential on the passive film formation as shown by chronoamperometric transients at 0.2 V and 0.4 V (Fig. 3) for iron electrodes in 0.3 M sulfate solution illustrates that pit formation is more difficult and precipitate products are formed at higher potentials. When the potential stepped from −1 to 1 V and maintains for 1 h at the latter value, the electrode experienced no localized attack and appeared golden and shiny, indicating the surface film growth. It shows the optical phenomenon of multiple thin layer light beam interference [34] and can be related to the existence of a hydrous iron oxide layer which is yellow–green at positive potentials [35].

The voltammogram for the iron electrode in bicarbonate solution only shows an oxidation current peak at about −0.6 V (Fig. 6), which is ascribed to the onset of the formation of solid oxides species on the electrode surface. The dissolution current is of three orders of magnitude lower with the passivation region being 400 mV wider than that of the iron electrode in a sulfate solution with the same concentration. The electrochemical behaviour of iron in bicarbonate solution is similar to the one for borate solution but the current is larger [36]. It is worth noting that the buffer capacity of bicarbonate solution is weaker than that of borate solution which influences the involved chemical and electrochemical reactions. In the active dissolution region, iron dissolves as an unstable $FeHCO_3^+$ complex [37] and at the anodic current peak (−0.6 V), $FeCO_3$ ($FeCO_3\,K_{sp} = 3.07 \times 10^{-11}$) [38] starts to precipitate [39]. As the positive potential increases, $FeCO_3$ may be transformed to an oxide, and the oxidation state of the iron species in the passive layer changes. The surface enhanced Raman spectrum [39] of the film formed at −400 mV and at 0 V is different from each other. The spectra at −400 mV indicate the presence of $Fe(OH)_2$ as well as $FeCO_3$, but when the potential subsequently steps to 0 V, the peaks associated with $FeCO_3$ are absent. In the passive film, the oxidation of $Fe^{2+}$ to $Fe^{3+}$ passes by a green rust transient ($[Fe_4(II)$-$Fe_2(III)(OH)_{12}][CO_3.\,2H_2O]$) between ferrous hydroxides and ferric oxyhydroxides [20]. The composition of transient compounds changes with the ratio of $Fe^{2+}/OH^-$.

The bicarbonate ions participate in the kinetics of oxidation in the transpassive region and it is possible to separate the processes corresponding to the formation of Fe(VI) species and the oxygen evolution reaction. It was discussed in the literature [28–30] that the $OH^-$ concentration markedly influences the production of $FeO_4^{2-}$ and that the free ferrate in solution decomposes at a higher rate than the surface Fe(VI) complex. The anodic plateau current (Fig. 6) illustrates that the presence of bicarbonate/carbonate ions in the solution stabilizes ferrate in the surface film. In the study of mild steel [40] and 304 stainless steel [41] in bicarbonate solutions, a current plateau in the transpassive region was also reported and attributed to the generation of ferrate species. In the case of iron in borate and sulfate solutions at the same pH, the anodic current increased with the onset of oxygen evolution and no ferrate formation was observed.

Voltammograms of iron in solutions containing both sulfate and bicarbonate ions are characterized by the presence of two anodic peak currents in two separate potential regions (Fig. 7). The addition of more $NaHCO_3$ to $Na_2SO_4$ solutions resulted in a substantial increase for peak current I, a decrease for

*Table 1. Summary of the observed results for an iron electrode in aqueous solution of bicarbonate and sulfate ions*

| $NaHCO_3/Na_2SO_4$ molar ratio | Corrosion type | Active–passive dissolution region /V | Localized attack region /V | Passivation region /V | Transpassive region /V |
|---|---|---|---|---|---|
| $NaHCO_3$ only | uniform | −0.85 to −0.4 | no | −0.4 to 0.9 | >0.9 (ferrate) |
| >10 : 1 | uniform | −0.85 to −0.4 | no | −0.4 to 0.9 | >0.9 (ferrate) |
| <10 : 1 | pitting | −0.85 to 0.4 | −0.1 to 0.4 | 0.4 to 0.9 | >1.0 (ferrate) |
| $Na_2SO_4$ only | uniform | −0.85 to 0.3 | no | 0.3 to 1.2 | >1.2 (no ferrate) |

peak current II and potential range increase for the passive region (Figs 9 and 10). The anodic peak currents I and II are most likely related to the formation of soluble $FeHCO_3^+$ complex and green rust 2 (GR2), respectively. SERS studies show that the films formed on iron in mildly alkaline solutions of nitrate, carbonate/bicarbonate, sulfate and borate are similar [39]. The rate of iron oxidation in sulfate and nitrate is greater than that in carbonate/bicarbonate which is, in turn, greater than that in a borate buffer. The major constituents for all solutions are similar and it is suggested that the effect of the anions on the rate of oxidation of iron in mildly alkaline solutions results from their abilities to form soluble complexes with either $Fe^{2+}$ or $Fe^{3+}$ [39].

A different electrochemical behaviour for iron in sulfate solutions and chloride solutions containing inhibitive ions has been reported in the literature [9, 10]. The main difference is that for iron in a chloride solution after pit initiation, the current increases markedly and does not show any inhibition potential, indicating that the pitting corrosion products are not protective because of their high solubility. For sulfates, the increasing concentration of dissolution products in the pits during pitting corrosion results in the precipitation of corrosion products which further hinder the pitting growth process. With an ionic radius of 8 : 1 for sulfate to chloride [38], it is deduced that sulfate ions have less mobility than chloride ions to leave the pit sites. In the presence of aggressive ions when an appropriate pH is attained at the surface, sulfate ions can adsorb and react with the passive layer and later with metallic iron. Since sulfate ions adsorb better than carbonate ions [42], sulfate ions compete with carbonate species and cause pitting. When pitting products cover the pits, these reactions slow down and local passivation starts. When pitting manifests, it causes a potential drop inside the pits shifting the potential inside the pits to the active dissolution region and accelerate the dissolution rate [43]. In accordance with the existence of green rusts, depending on the ratio of $Fe^{2+}/OH^-$ during the dissolution reactions and changes in the surface pH, different transient compounds can be formed. However, in such a case, there is competition between sulfate and carbonate species. It has been found that these transient compounds have a different selectivity towards sulfate and carbonate ions and their tendency is more toward carbonate than sulfate ions [44]. Hence, as transient compounds form on the surface with an accumulation of carbonate species on the electrode surface, the current starts to decrease and passivation begins.

The type of corrosion noticed in the present investigations is summarized in Table 1 for the bicarbonate/sulfate ions molar ratio.

## Acknowledgements

Gh. Vatankhah gratefully acknowledges the Ministry of Culture and Higher Education (MCHE) of Iran for his graduate scholarship. The authors also acknowledge the financial support of Hydro-Québec (IREQ), and Natural Sciences and Engineering Research Council of Canada (NSERCC).

## References

[1] N. Sato, *Corros. Sci.* **37** (1955) 1947 and the references therein.
[2] M. Yamaguchi, H. Nishihara and K. Aramaki, *ibid.* **37** (1995) 571.
[3] Y. T. Chin and B. D. Cahan, *J. Electrochem. Soc.* **139** (1992) 2432.
[4] R. D. Grimm, A. C. West and D. Landolt, *ibid.* **139** (1992) 1622.
[5] K. Cho and H. W. Pickering, *ibid.* **138** (1991) L56.
[6] J. A. Bardwell and B. MacDougall, *ibid.* **135** (1988) 2157.
[7] V. Jovancicevic, J. O'M. Bockris and J. L. Carbajal, *J. Electrochem. Soc.* **133** (1986) 2219.
[8] T. Zakroczymski, C. J. Fan and Z. Szklarska-Smialowska, *ibid.* **132** (1985) 2868.
[9] Z. Szklarska-Smialowska, 'Pitting Corrosion of Metals', NACE, Houston, TX (1986).
[10] P. Marcus and J. Oudar (Eds), 'Corrosion Mechanisms in Theory and Practice', Marcel Dekker, New York (1995).
[11] Z. Szklarska-Smialowska, *Corros. Sci.* **18** (1978) 97.
[12] J. F. Marco, J. R. Gancedo, N. Meisel, P. Griesbach and P. Gütlich, *Corrosion* **47** (1991) 498.
[13] H. E. H. Bird, B. R. Pearson and P. A. Brook, *Corros. Sci.* **28** (1988) 81.
[14] T. Kodama, *Boshoka Gijutso* **23** (1974) 5.
[15] B. MacDougall and J. A. Bardwell, *J. Electrochem. Soc.* **135** (1988) 2437.
[16] J. Gui and T. M. Devine, *Corros. Sci.* **36** (1994) 441.
[17] C. A. Acosta, R. C. Salvarezza, H. A. Videla and A. J. Arvia, *ibid.* **25** (1985) 291.
[18] B. G. Pound, G. A. Wright and R. M. Sharp, *Corrosion* **45** (1989) 386.
[19] M. Abdelmoula, Ph. Refait, S. H. Drissi, J. P. Mihe and J. M. R. Génin, *Corros. Sci.* **38** (1996) 623.
[20] S. H. Drissi, Ph. Refait, M. Abdelmoula and J. M. R. Génin, *ibid.* **37** (1995) 2025.
[21] Ph. Refait, M. Abdelmoula and J. M. R. Génin, *ibid.* **36** (1994) 55.
[22] A. A. Olowe and J. M. R. Génin, *ibid.* **32** (1991) 965.
[23] A. A. Olowe, B. Pauron and J. M. R. Génin, *ibid.* **32** (1991) 985.
[24] A. A. Olowe, Ph. Refait and J. M. R. Génin, *ibid.* **32** (1991) 1003.
[25] A. A. Olowe and J. M. R. Génin, *ibid.* **32** (1991) 1021.

[26] *Idem*, CEBELCOR RT297 (1989), p. 363.
[27] W. J. Lorenz and K. E. Heusler, 'Corrosion Mechanisms' (edited by F. Mansfeld), Marcel Dekker (1987).
[28] F. Beck, R. Kauss and M. Oberst, *Electrochim. Acta* **30** (1985) 173.
[29] C. M. Rangel, R. A. Laitão and I. T. Fonseca, *ibid.* **34** (1989) 255.
[30] C. M. Rangel, I. T. Fonseca and R. A. Laitão, *ibid.* **31** (1986) 1659.
[31] J. G. N. Thomas, A. D. Mercer and J. D. Davies, Proceedings of the International Conference on Corrosion Inhibition (edited by R. H. Heusler) (1983), p. 89.
[32] D. B. Gibbs and M. Cohen, *J. Electrochem. Soc.* **119** (1972) 416.
[33] M. Pourbaix, 'Atlas of Electrochemical Equilibria in Aqueous Solutions', NACE, Houston, TX (1974).
[34] S. Tolansky, 'Multi-beam Interference Microscopy of Metals', Academic Press, New York, (1970).
[35] L. D. Burke and M. G. Lyons, *J. Electroanal. Chem.* **198** (1986) 347.
[36] K. Ogura and K. Sato, 'Passivity of Metals' (edited by R. P. Frankental and J. Kruger), The Electrochemical Society Corrosion Monograph Series, Princeton, NJ (1978), p. 443.
[37] E. B. Castro, J. R. Vilche and A. J. Arvia, *Corros. Sci.* **32** (1991) 37.
[38] 'CRC Handbook of Chemistry and Physics', 71st. edn, CRC Press, Boca Raton (1990–1991).
[39] J. Gui and T. M. Devine, *Corros. Sci.* **37** (1995) 1177.
[40] S. Simard, M. Drowgaska, L. Brossard and H. Menard, *J. Appl. Electrochem.*, **27** (1997) 317.
[41] M. Drowgaska, L. Brossard and H. Menard, *J. Appl. Electrochem.* **26** (1996) 217.
[42] Ya. M. Kolotyrkin, R. M. Lazorenko-Manevich and L. A. Sokolva, *J. Electroanal. Chem.* **228** (1987) 301.
[43] H. W. Pickering, *Corros. Sci.* **29** (1989), 325.
[44] A. Mendiboure and R. Schöllhorn, *Revue de Chimie Minérale* **23** (1986) 819.